24th COBEM - 2017

24th ABCM International Congress of Mechanical Engineering
December 3-8, 2017, Curitiba, PR, Brazil

# COBEM-2017-2830
# CERAMICS CUTTING TOOLS APPLY ON DRY TURNING OF GRAY AND NODULAR CAST IRON

**José Vitor Cândido de Sousa**
**Taíse Azevedo de Sousa**
**Elson de Campos**
**Marcos Valério Ribeiro**
[1]*São Paulo University (Unesp), School of Engineering, Guaratinguetá – SP, Brazil* ;
candido@feg.unesp.br;
taiseazevedo.sousa@yahoo.com.br;
elson@feg.unesp.br;
mvalerio@feg.unesp.br

**Olivério M. M Silva**
oliverio.silva@bil.com.br
[2]*DCTA-IAE/AMR - Pça. Marechal do A. E.Gomes, 50, S. J. Campo s - SP, CEP. 12228-904,*

*Abstract: The goal of this work was to compare the cutting performance of the alumina ($Al_2O_3$) and silicon nitride ($Si_3N_4$) inserts under dry cutting environment on nodular and gray cast iron using the cutting speed ($V_c$) of 500 m/min, feed rate (f) of 0.25 and 0.33 mm/rev and depth of cut ($a_p$) of 0.50 and 1.0 mm respectively. Tools performance was evaluated with respect at tool wear, temperature, surface finish produced and cutting forces generated during dry turning, using light optical microscopy (LOM), non-contact infrared pyrometer, surface roughness meter and dynamometer with data acquisition system respectively. Higher micro hardness of silicon nitride samples (1760 HV) compared to alumina (1530 HV) is observed and depicts better resistance against abrasion. The tool life of $Si_3N_4$ insert is found to be better than the $Al_2O_3$ insert with cutting length above of 10500 meters. The dominant wear mechanism was found to be abrasion with progression of wear was steady. In the general, we can attribute the favorable cutting performance of cutting to effect positive of graphite as solid lubrificant, besides of the research have shown high efficiency of dry cutting due to not harmful to the environment in comparison with traditional technologies using cutting fluids.*

***Keywords:*** *$Si_3N_4$ and $Al_2O_3$ cutting tools; Flank wear; Gray cast iron; Nodular cast iron.*

## 1. INTRODUCTION (TIMES NEW ROMAN, BOLD, SIZE 10)

Innovative ceramic engineering over the past decades on high-temperature structural ceramics has resulted in an impressive array of high-performance ceramic cutting tools which have had a major positive impact in machining process and production efficiency. The industry is the key driver for the development of ceramics cutting tool materials to machine difficult-to-cut materials and to improve a high finished product. Ceramics cutting tools offer high productivity due to their hardness, chemical inertia and abrasion resistance, which allows their use in dry machining process and at high cutting speeds. However, the difficulty in the using these tools in the market is related to their possible fragility, kinds of tool machines, and others [1-2]. Among at ceramic cutting tools, the alumina (Al2O3) is one of the most abundant ceramic materials and a well-known oxide material which has been used as refractory or technical ceramic. However, the low fracture toughness, in order of 2MPam1/2, limits its application [3-4]. Another ceramic the silicon nitride is one of the most promising structural materials due to their high hardness, wear resistance and chemical stability, especially where the temperature of the tool tip can reach up to 1200ºC depending on the type of the machined metal during a machining operation. The negative effect of the weak grain boundary glassy phase on the high-temperature mechanical properties of the β-Si3N4 material at these temperatures can be overcome by incorporating the liquid phase into the Si3N4 structure [5, 6]. The high-speed machining has been widely used in aerospace and automotive industry because of its lower cutting cost and good mechanical properties of the cutting tools [7]. Therefore, the mechanical properties of cutting tools become the key factors to ensure the machining efficiency. Ceramic cutting tools have already been widely used for machining hard materials due to their unique mechanical properties [8-9].

## 2. EXPERIMENTAL PROCEDURE

### 2.1. Material testing

Two kinds of ceramics cutting (Al2O3 and Si3N4) inserts were chosen to investigate in this study. The density was measured by Archimedes' method in distilled water. The cross-section of cutting inserts was mirror polished and then indented with 98 N load for 10 s by Vickers hardness tester with a diamond Vickers indenter at room temperature. At least ten indentations were made for each insert. The hardness and fracture toughness of the cutting inserts were calculated according to ASTM C1327-15 [10], and ASTM C 1421-10 [11] respectively. Phase composition of the cutting inserts was characterized by X-ray diffraction (XRD), with Cu-Kα radiation within scanning range between 20ºand 80º, angular step of 0.05º (3s/point). Relative density was obtained by a relation between apparent density (Archimedes' method) and real density of Al2O3 and Si3N4 (obtained by He-pycnometer), the microstructure was observed in a Hitachi-TM3000 SEM.

### 2.2. Dry cutting performance

All experiments were carried out on a computer numerical control (CNC) lathe (Romi, Mod. Centur 30D) under dry cutting condition using Al2O3 and Si3N4 cutting tools the comparison, according to ISO 1832:2004. The ISO code of the tool holder is CSRNR 2525 M 12CEA type (offset shank with 15 [75º] side cutting edge angle, 0º insert normal clearance and 25 mm x 25 mm x 150 mm) was used for the cutting experiments. The cutting performance of Si3N4 cutting tool was tested on dry turning using a pearlitic grey cast iron bars GG25 (DIN1691) with 3.0% carbon, 2.0% silicon and 0.6% manganese, the tensile strength is 245–290 MPa, hardness varies from 205–230HB and fatigue strength 100 MPa. The nodular cast iron (FUCO FE45012) bars, 104x300mm (diameter/length), composed of nodular graphite in duplex ferritic/perlitic matrix (hardness of 220HB) and nominal chemical composition 3.15±0.1wt.%C, 2.5±0.1wt.%Si, 0.4wt.%Mn, 0.5±0.05wt.%P, 0.6±0.05wt.%S, 0.05±0.01wt.%Cr, 0.1±0.05wt.%Cu, and iron chemical balance. In order to guarantee the initial surface roughness, a pre-machining was made to remove the cast skin in everything workpieces. During the turning process, the two cutting inserts have a shape of SNGN120712 (12.7 mm × 12.7 mm × 7.94 mm) with rε=0.8 mm, bγn=0.20 mm, γnc=-20°. The cutting speed (Vc) of 500 m/min, feed rate (f) of 0.25 and 0.33 mm/rev and depth of cut (ap) of 0.50 and 1.0 mm to nodular and gray cast iron respectively. The density and mechanical properties of the cutting inserts were given in Table 1. For each pass was used twice repeated with based on recent work of Souza, (2009) [9]. Initially, the work material had a cylindrical shape, with 105 mm in diameter and 305 mm cutting length. For meeting this goal the each test was started with a fresh cutting edge with at machining was stopped until determinates cutting lengths. Tool wear measurements were performed on optical tool maker microscope with removing the inserts out of the cutter to measure the surface roughness of work piece, flank and crater wear on the tool. Three surface roughness measurements were taken, distant from each other by 120° in the cylindrical work material using a surface roughness meter (Mitutoyo Surftest 402 series 178). The average temperature was measured with a non-contact infrared pyrometer, with laser dot sighting pointed in the cutting nose fixed in the carriage at 20 cm from cutting edge, agreement Souza, et al. (2009) [9]. For each pass, the average and standard deviation surface roughness and temperature were calculated. The three forces component analogue dynamometer was used in order to measure of the main cutting force (Fc) (in tangential direction to the bar), feed force (Ff) (in axial direction) and Thrust force (Ft) (in radial direction) in longitudinal turning tests were converted and filtered in real time using dedicated software in a computer connection for data acquisition was also made and calibrated.

**Table 1**: Density and mechanical properties of the $Y_3Al_5O_{12}$ and β-$Si_3N_4$ cutting inserts.

| **Inserts** | **Relative density (%)** | **Mechanical properties** | |
|---|---|---|---|
| | | Hardness HV10/GPa | Fracture toughness Mpa.$m^{1/2}$ |
| $Al_2O_3$ | 98.3%±0.40 | 15.30±0.31 | 4.6±0.40 |
| $Si_3N_4$ | 98.20±0.13 | 17.60±0.23 | 5.10±0.18 |

## 3. RESULTS AND DISCUSSION

### 3.1. Properties and microstructures

Two XRD patterns of the cutting inserts are shown in Fig. 1 (a-b). It can be seen that the main phases of the two cutting inserts are all $Y_3Al_5O_{12}$ and β-$Si_3N_4$.

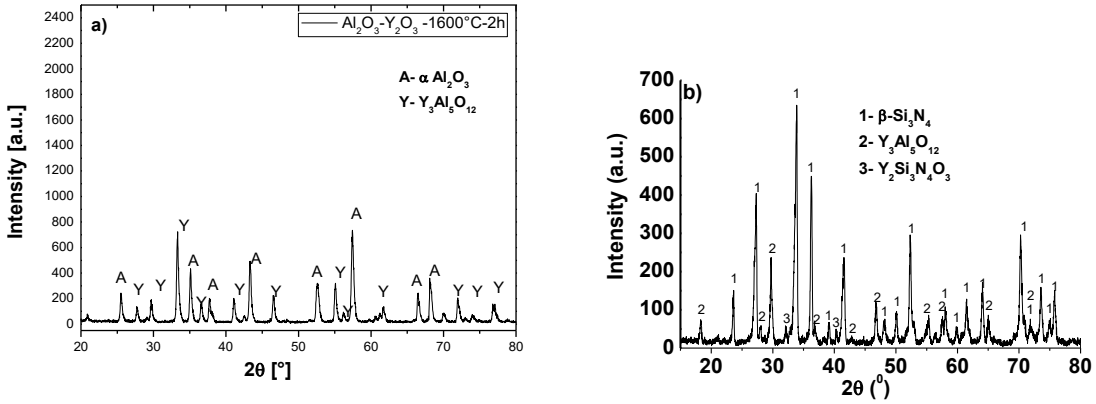


**Figure 1: (a-b)** presents the XRD pattern and SEM micrographs of sintered $Al_2O_3$-YAG and $Si_3N_4$-additives composite.

**Figure 1 (a)** showed the presence of α-$Al_2O_3$ and $Y_3Al_5O_{12}$ as crystalline phases, indicating that $Y_2O_3$ present in powders mixtures was converted into $Y_3Al_5O_{12}$ by stoichiometric reaction in solid state, between $Y_2O_3$ and $Al_2O_3$. The YAG formation that happens simultaneously with sintering stages the solid state apparently promoted an increasing on $Al_2O_3$-sinterability, reaching a relative density of 98.3%±0.4, whose results are superior to the ones found in literature for monolithic alumina sintered in similar condition to the ones experimented in this work [12-14]. **Figure (1b)** showed the presence of α to β-$Si_3N_4$ phase transformations were completed after the sintering. The main secondary crystalline phases were detected in the cutting tool ($Y_3Al_5O_{12}$ and $Y_2Si_3N_4O_3$) due to the composites containing Y, Ce and Al as the additives. In addition, the chemical reactions create a $SiO_2$ based film on silicon nitride particles with $O_2$ contact. In Table 1 illustrates the relative density of pressuring sintering of β-$Si_3N_4$ compacts at 1850 ºC for 2 h under a pressure of 0.1 MPa with $Y_2O_3$–$CeO_2$–AlN–$Al_2O_3$ addition. Fig2. (c-d) shows the microstructures of the cutting inserts.

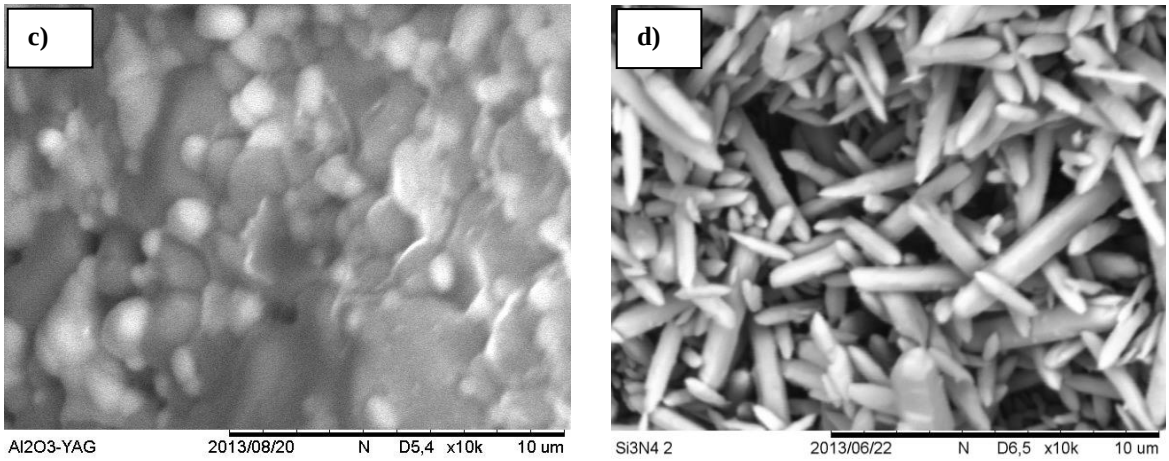


**Figure 2: (c-d)** SEM micrographs of sintered $Al_2O_3$-YAG and β-$Si_3N_4$ tools.

Obviously, it can be seen that both cutting inserts mainly contain equiaxed and elongated grains. In SEM micrographs, **Figure 1c**, it is observed two phases well distributed along the microstructure. The white phase represents $Y_3Al_5O_{12}$ and it appears surrounding the $Al_2O_3$ matrix (gray grains). A homogeneous phase-distribution is essential for the composite to perform its role positively as increasing the machining tool life cycles, guaranteeing the reproducibility of its properties during machining. In the **Figure, 1d**, can be observed that the distributions of grains size and their area fraction showed bimodally. The microstructures of $Si_3N_4$ sample present elongated needle-like β-$Si_3N_4$ grains surrounded by secondary phase (see Fig. 1b). This elongated β–$Si_3N_4$ grains have a positive influence on the fracture resistance of the cutting tool. The dark field area represents the secondary phases it confirms the amounts of secondary phases were also visibly with significant grain growth and isolated grain boundary pockets.

Table 1 shows the physical and mechanical properties of $Y_3Al_5O_{12}$ and β-$Si_3N_4$ samples. The densities of the α-$Al_2O_3$ and $Y_3Al_5O_{12}$ and β–$Si_3N_4$ are 98.3%±0.40 and 98.20±0.13, respectively. As can be seen, the densities of two cutting tools are very similar, even though the phase composition of α-$Al_2O_3$ and $Y_3Al_5O_{12}$ is quite different from β–$Si_3N_4$ (Fig. 1a-b). It is obviously seen that the different hardness value. The Vickers hardness of β-$Si_3N_4$ cutting tool ceramics presents important value of 17.60 GPa. This value can be considered as the medium value due to the partial $Y_2O_3$ presence is related to its higher content of β-$Si_3N_4$ grains. The results were in function of higher relative density, possible large grain size and increase in intergranular phase cause large indent area. Normally the formation of interlocked structures with some elongated β-$Si_3N_4$ structure may increase the fracture toughness the material. The shared addition of $Y_2O_3$ and $CeO_2$ the intergranular phase to increased and promote fracture toughness of 5.10±0.18 Mpa.$m^{1/2}$.

For α-$Al_2O_3$ and $Y_3Al_5O_{12}$ the Vickers Hardness and fracture toughness were 15.20±0.3GPa and 4.6±0.4MPa.$m^{1/2}$, respectively. The hardness of 20GPa and fracture toughness between 2 and 3MPa.$m^{1/2}$ are resulted commonly found for monolithic-$Al_2O_3$ tools. The decrease of hardness values limits the range of applications for this $Al_2O_3$-YAG tool in refractory-metals machining, however, the high densification levels and higher fracture toughness obtained in this work can be beneficial for machining less resistant metals as nodular cast iron.

### 3.2. Tool life

Fig. 2 presents the flank wear width (VB) as a function of the machining length for $Al_2O_3$-YAG and β-$Si_3N_4$ cutting inserts the dry turning of nodular and gray cast iron respectively. As can be seen, the β-$Si_3N_4$ tool lasted longer than the $Al_2O_3$ ceramic tool. The difference in life between $Si_3N_4$ and $Al_2O_3$ ceramic tools was more than 2 fold at the highest.

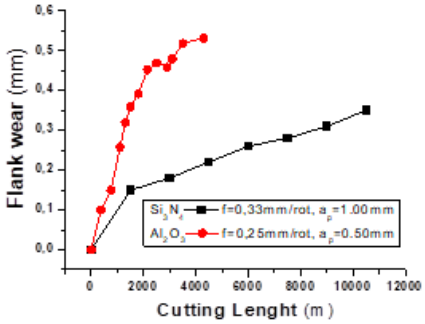


**Fig 2: (a).** Flank wear of the $Al_2O_3$-YAG and β-$Si_3N_4$ inserts as a function of the cutting length

It can be seen that the VB of $Al_2O_3$-YAG is larger than that of β-$Si_3N_4$ at the cutting speed of 500m/min. However, the biggest difference between cutting tools can be in function of different feed rate (f) of 0.25 and 0.33 mm/rev and depth of cut ($a_p$) of 0.50 and 1.0 mm respectively because β-$Si_3N_4$ exhibits better wear resistance than $Al_2O_3$-YAG as the cutting speeds same. It is known that the hardness of β-$Si_3N_4$ is higher than that of $Al_2O_3$-YAG from above discussion. Therefore, the wear rate of β-$Si_3N_4$ decreasing can be attributed to the fact that graphite particles →decrease friction on the tool/workpiece interface and between the tool and chip due to their natural solid lubricant character.

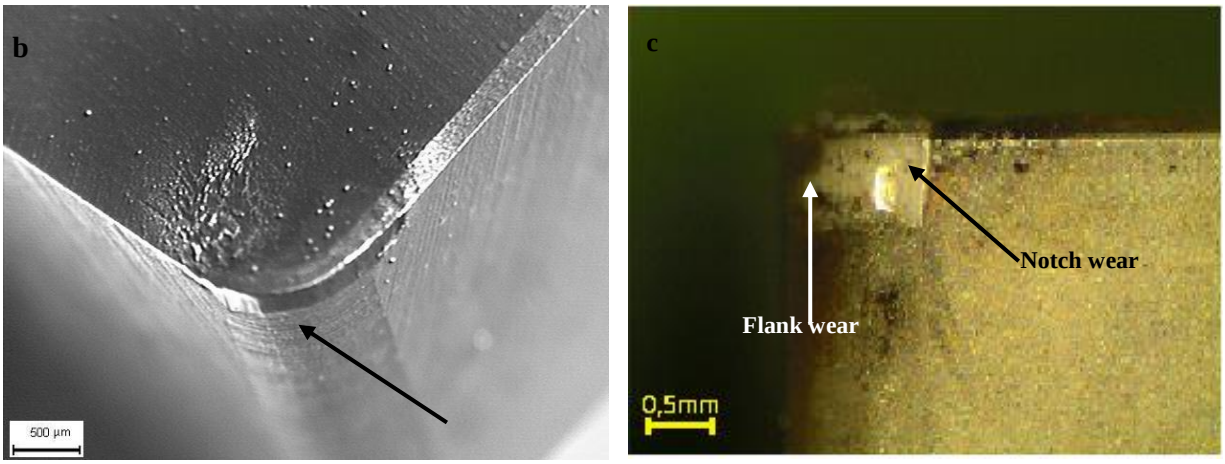


**Fig 2: (b-c).** Flank wear: **b)** β-$Si_3N_4$: f=0.33mm/rot, $a_p$=1.00; **c)** $Al_2O_3$-YAG: f=0.25mm/rot, ap=0.5mm.

Light optical microscopy (LOM) images taken from the flank worn surfaces of the cutting inserts after cutting tests are shown in Figs. 2b-c). It can be seen that the wear band of β-$Si_3N_4$ and $Al_2O_3$-YAG is uniform with light abrasive tracks on worn surface. It indicates that the dominant wear mechanism is mainly abrasive wear, accompanied by minor adhesive wear. When cutting gray and nodular cast iron in these conditions.

It was written "more than" because the $Si_3N_4$ tool did not reach the wear criterion adopted for the end of tool life (VB= 0.6mm); therefore, the experiments with this tool were interrupted when they reached 35 min of cutting time. It because the $Si_3N_4$ tool showed the hardness of 1760 HV at room temperature while the hardness of $Al_2O_3$ tool is 1500 HV. The higher Vickers hardness, it helps to outcome positive can be attributed to the fact that graphite particles decrease friction on the tool/workpiece interface and between the tool and chip due to their natural solid lubricant character. The results also indicate that, for the turning of gray cast iron and nodular cast iron at varying feed rate (*f*) of 0.25 and 0.33 mm/rev and depth of cut ($a_p$) of 0.50 and 1.0 mm respectively, the wear mechanism was highly consistent for the $Al_2O_3$-YAG and the β-$Si_3N_4$ cutting inserts. But it is also possible that diffusion abrasion of minor elements occurs during the cutting process.

### 3.3. Cutting temperature

The temperature generation in the dry turning nodular and gray cast iron was determined from the measured temperature distribution along the tool-workpiece interface for a set cutting length value. Unlike flank wear, the temperature does not always continuously increase with increasing cutting length. Many other factors besides flank wear may have some effect on the cutting temperature, for instance, inhomogeneity of nodular cast iron, random distribution of graphite nodules, mechanical properties punctual, cutting tool microstructure, machining parameters, etc.

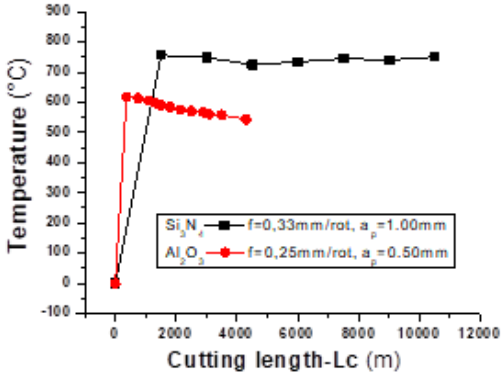


**Figure 3:** Temperature vs. cutting length

In **Figure 3**, it is observed that temperature in $Al_2O_3$-YAG tool is slightly lower than β-$Si_3N_4$ tools at long of cutting length, remaining around 543°C while β-$Si_3N_4$ tool presented temperature of 750°C. **Figure 3** showed that during dry machining tests there was a decreasing temperature at the end of tool-workpiece interface and confirms that the initial contact temperatures to $Al_2O_3$-YAG tool were higher than those of later machining states. For β-$Si_3N_4$ tool can be observed that during the dry machining trials, the average interface temperature almost constant changes from 756°C to 750°C. The results highlight the pertinence of updating the contact parameters such as the pressure and the interfacial temperature area while the geometry of the tool rake faces changes.

### 3.4. Surface roughness

It is probably because the ceramic cutting tools in machining process after a few minutes promoted a better compromise between the tool and the workpiece with possible vibrations reduced. In the Figure 4 (a-b) can been observed which the flank geometric allows a better accommodation between tool and workpiece. However, this fact to alone is not sufficient to reduce the surface roughness, but can facilitate the accommodation among cutting tools, workpiece and chip due to possibly natural deposition of graphite in interface in function of heat generated by abrasive contact. Absorption of graphite in this region promote better machinability due to the low friction coefficient generated that promote easy chip remove of the workpiece surface.

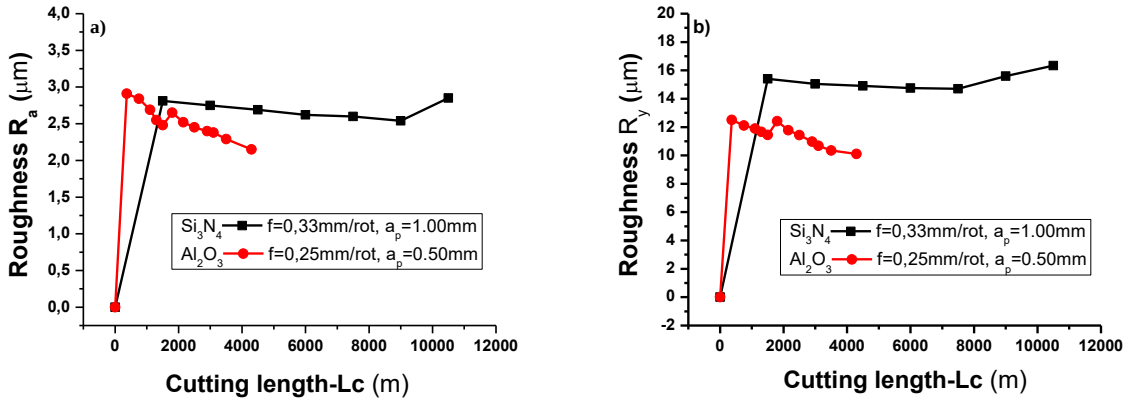


**Figure 4:** a) Surface roughness $R_a$; b) Surface roughness $R_y$ as a function of cutting length.

The results showed that the increase in feed rate increases surface roughness is shown in **Figure 4**. This is due to distinct feed marks produced by the cutting edge. As the feed rate increases there is a little or no thermal softening occurs at the feed rates of 0.33 mm/rev which leads to more tearing and high surface roughness. In a general way, pieces machined with $Al_2O_3$-YAG, present roughness, $R_a$ of 2.15µm and $R_y$ of 10.11µm, while those machined with β-$Si_3N_4$ present $R_a$ of 2.85µm, and $R_y$ of 16.34µm varying feed rate (*f*) of 0.25 and 0.33 mm/rev and depth of cut ($a_p$) of 0.50 and 1.0 mm respectively.

### 3.5. Cutting forces

In the experiments, the dynamometer directly measures the *x*, *y* and *z* direction forces, which are Cutting force – Fc, Thrust force – Ft and Feed force – Ff in longitudinal dry turning tests. Typical results obtained for the cutting force versus cutting length are shown in Fig.5. The knowledge of cutting force is very important in dry machining operations because they have a strong relationship with cutting performance such as surface finish, dimensional accuracy, tool life and cutting temperature.

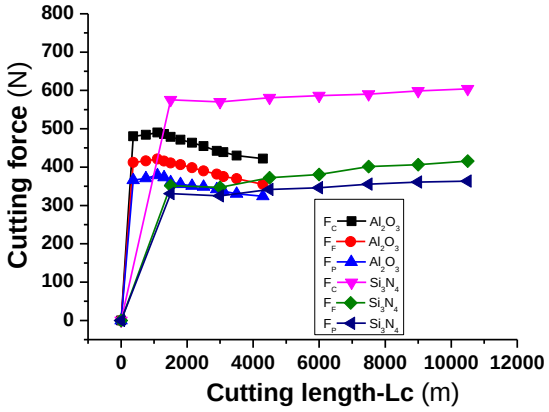


**Fig. 5** : Variation of cutting forces versus cutting length.

Effect of the cutting tools types can be seen from the **Figure 5** that all three components of cutting forces change significantly with the increase of cutting time. The cutting force measurements showed lower cutting forces for the $Al_2O_3$-YAG cutting tool compared to the β-$Si_3N_4$, which was true especially for the $V_c$= 500m/min. Using $Al_2O_3$-YAG cutting tool the effect of feed rate (*f*) of 0.25mm/rev at 500 m/min the measured cutting forces decreased. From the Figure 5 can be seen that the cutting force (Fc) component was greater than the thrust force component by a considerable margin. This result indicates that the material removal has occurred in a ductile manner.

However, in this study, a decrease is observed in the main cutting force at $V_c$=500 m/min with feed rate (*f*) of 0.25mm/rev and depth of cut ($a_p$) of 0.50 mm it is considered that the forces distribution in flank edge, rake face and area vicinity at the cutting tool due to high temperatures of shear area. Under high cutting temperature, the graphite material may be softening, released and smeared on the tool rake and flank face, and resulted in a decrease in friction coefficient due to more effective film formation.

## 4. CONCLUSION

The results are enticing to application industrial and analytical perspectives aimed at indicating science and technologic that exist a condition feasible to instructing the optimization of machining processes.

We can observe that effect of the cutting tools can be seen all three components of cutting forces change significantly with the increase of cutting time, a decrease is observed in the main cutting force at Vc=500 m/min with feed rate (f) of 0.25mm/rev and depth of cut (ap) of 0.50 mm

## 4. REFERENCES

[1] R. Lach, K. Wojteczko, A. Dudek, Z. Pedzich, Fracture behaviour of alumina-YAG particulate composites, J. Eur. Ceram Soc, 34 (2014) 3373–3378.
[2] T.A. Parthasarathy, T. Mah, L.E. Matson, Processing, structure and properties of alumina–YAG eutectic composites, J Ceram Process Res, 5 (2004) 380-390.
[3] F.J. Paneto, J.L. Pereira, J.O. Lima, E.J. Jesus, L.A. Silva, E. Sousa Lima, R.F. Cabral, C. Santos, Effect of porosity on hardness of Al2O3–Y3Al5O12 ceramic composite , Int. J. Refract. Metals Hard Materials, 48 (2015) 365–368.
[4] N. Camus_cu, Effect of cutting speed on the performance of Al2O3 based ceramic tools in turning nodular cast iron, Materials and Design, 27 (2006) 997–1006.
[5] Souza, J.V.C.; Nono, M.C.A.; Ribeiro, M.V.; Machado, J.P.B.; Silva, O.M.M. Cutting forces in turning of gray cast iron using silicon nitride based cutting tool, Materials & Design, v.30, (2009), pp. 2715-2720.
[6] Souza, J. V. C.; Silva, O. M. M.; Nono, M. C. A.; Machado., J. P. B.; Pimenta, M.; Ribeiro, M. V.; Si3N4 ceramic cutting tool sintered with CeO2 and Al2O3 additives with AlCrN coating. Materials Research, v. 14, 2011, p. 514-518.
[7] Y. long, J. Zeng, D. Yu, et al., Microstructure of TiAlN and CrAlN coatings and cutting performance of coated silicon nitride inserts in cast iron turning, Ceram. Int. 40 (2014) 9889–9894.
[8] J. Qin, Y. Long, J. Zeng, et al., Continuous and varied depth-of-cut turning of gray cast iron by using uncoated and TiN/Al2O3 coated silicon nitride-based ceramics tools, Ceram. Int. 40 (2014) 12245–12251.
[9] J.V.C. Souza, M.C.A. Nono, M.V. Ribeiro, et al., Cutting forces in turning of gray cast iron using silicon nitride based cutting tool, Mater. Des. 30 (2009) 2715–2720.
[10] ASTM C1327-15. Standard test method for Vickers indentation hardness of advanced ceramics (2015).
[11] ASTM C1421-10. Standard test method for determination of fracture toughness of advanced ceramic at ambient temperature (2010).
[12] F.J. Paneto, J.L. Pereira, J.O. Lima, E.J. Jesus, L.A. Silva, E. Sousa Lima, R.F. Cabral, C. Santos, Effect of porosity on hardness of Al2O3–Y3Al5O12 ceramic composite , Int. J. Refract. Metals Hard Materials, 48 (2015) 365–368.
[13] N. Camus_cu, Effect of cutting speed on the performance of Al2O3 based ceramic tools in turning nodular cast iron, Materials and Design, 27 (2006) 997–1006.
[14] B. Yao, H. Su, J. Zhang, Q. Ren, W. Ma, L. Liu, H. Fu, Sintering densification and microstructure formation of bulk Al2O3/YAG eutectic ceramics by hot pressing based on fine eutectic structure, Materials and Design, 92 (2016) 213–222.

## 5. RESPONSIBILITY NOTICE

The author(s) is (are) the only responsible for the printed material included in this paper.